EUROPEAN ORGANIZATION FOR NUCLEAR RESEARCH

CERN-EP/99-145
October 13, 1999

Search for Neutral Higgs Bosons of the Minimal Supersymmetric Standard Model in e^+e^- Interactions at $\sqrt{s} = 189$ GeV

L3 Collaboration

Abstract

A search for the lightest neutral scalar and neutral pseudoscalar Higgs bosons in the Minimal Supersymmetric Standard Model is performed using 176.4 pb^{-1} of integrated luminosity collected by L3 at a center-of-mass energy of 189 GeV. No signal is observed, and the data are consistent with the expected Standard Model background. Lower limits on the masses of the lightest neutral scalar and pseudoscalar Higgs bosons are given as a function of $\tan\beta$. Lower mass limits for $\tan\beta > 1$ are set at the 95% confidence level to be $m_{\mathrm{h}} > 77.1$ GeV and $m_{\mathrm{A}} > 77.1$ GeV.

Submitted to *Phys. Lett. B*

Introduction

In the Minimal Supersymmetric Standard Model (MSSM) [1] two Higgs doublets are required, giving rise to five Higgs bosons: a charged scalar pair, $\mathrm{H}^{\pm}$; two neutral scalars, h and H; and a neutral pseudoscalar, A. Within this framework, the h and A are predicted to be the lightest Higgs particles and, therefore, the most likely to be observed at LEP. The two main production mechanisms are investigated in this letter:

$$\mathrm{e^+e^-} \rightarrow \mathrm{Z^*} \rightarrow \mathrm{hZ} \quad (1)$$
$$\mathrm{e^+e^-} \rightarrow \mathrm{Z^*} \rightarrow \mathrm{hA}. \quad (2)$$

Process (1) is very similar to the dominant Standard Model Higgs production mechanism, for which L3 has set a lower limit on the mass of the Higgs at 95.3 GeV [2]. The production rate for (1) is, in general, smaller than that of the Standard Model reaction, but this is compensated by the additional pair-production process (2).

Previous searches for the h and A bosons have been reported by L3 [3] and other experiments [4]. In this letter, our sensitivity to these particles is extended by including the data taken at $\sqrt{s} = 189$ GeV and by scanning over a larger MSSM parameter space.

Data and Monte Carlo Samples

The data were collected using the L3 detector [5] at LEP during 1998. The integrated luminosity is 176.4 pb^{-1} at an average center-of-mass energy of 188.7 GeV.

The signal cross sections and branching ratios are calculated using the HZHA generator [6]. For the efficiency studies, Monte Carlo samples of Higgs events are generated using PYTHIA [7] and HZHA. For the background studies, the following Monte Carlo programs are used: PYTHIA ($\mathrm{e^+e^-} \rightarrow \mathrm{q\bar{q}}(\gamma)$), KORALW [8] ($\mathrm{e^+e^-} \rightarrow \mathrm{W^+W^-}$), KORALZ [9] ($\mathrm{e^+e^-} \rightarrow \tau^+\tau^-$), PHOJET [10] ($\mathrm{e^+e^-} \rightarrow \mathrm{e^+e^-q\bar{q}}$), EXCALIBUR [11] ($\mathrm{e^+e^-} \rightarrow \mathrm{f\bar{f}'f''\bar{f}'''}$) and PYTHIA ($\mathrm{e^+e^-} \rightarrow \mathrm{ZZ}$ and $\mathrm{e^+e^-} \rightarrow \mathrm{Ze^+e^-}$). The number of simulated background events for the most important background channels is typically 100 times the number of collected data events. The Monte Carlo signals are 300 times the number of events expected to be observed with these luminosities.

The L3 detector response is simulated using the GEANT 3.15 program [12], which takes into account the effects of energy loss, multiple scattering and showering in the detector. The GHEISHA program [13] is used to simulate hadronic interactions in the detector.

Analysis Procedures

The search for hA and hZ production is carried out within a constrained MSSM assuming unification of the scalar fermion masses, the gaugino masses and the trilinear Higgs-fermion couplings at the GUT scale. This choice has little impact on the Higgs mass phenomenology but reduces significantly the number of free parameters. The universal scalar fermion mass m_0 and the gaugino mass parameter M_2 are fixed to 1 TeV. The Higgs mass parameter μ is set to -0.1 TeV. Two extreme scenarios are considered corresponding to maximal and minimal scalar top mixing as suggested in Reference [14]. The minimal mixing scenario corresponds to setting the trilinear Higgs-fermion coupling A to zero. Maximal scalar top mixing occurs at $A = \sqrt{6}$ TeV. A scan is then performed, in each mixing scheme, over the two remaining free parameters m_{A} and $\tan\beta$. For this search, the minimum value of $\tan\beta$ considered has been decreased from 1.0 to 0.7 and the minimum A mass considered has been decreased from 30 GeV to 10 GeV with respect to our previous publication. Values of m_{A} in the range $m_{\mathrm{A}} < 10$ GeV have been previously excluded at LEP [15].

The two Higgs production mechanisms, $\mathrm{e^+e^-} \rightarrow \mathrm{Z^*} \rightarrow \mathrm{hA}$ and $\mathrm{e^+e^-} \rightarrow \mathrm{Z^*} \rightarrow \mathrm{hZ}$, vary in relative importance as a function of $\tan\beta$. The production of hA is dominant at high $\tan\beta$, while hZ production is dominant at low $\tan\beta$. The description of the hZ analyses at $\sqrt{s} = 189$ GeV of the decay modes other than $\mathrm{hZ} \rightarrow \mathrm{b\bar{b}q\bar{q}}$ and $\mathrm{hZ} \rightarrow \mathrm{b\bar{b}}\tau^+\tau^-$ can be found in Reference [2]. The analyses for $\mathrm{hZ} \rightarrow \mathrm{b\bar{b}q\bar{q}}$ and $\mathrm{hZ} \rightarrow \mathrm{b\bar{b}}\tau^+\tau^-$ ($\tau^+\tau^-$ $\mathrm{q\bar{q}}$) used in this letter have been optimized to account for the analogous signatures in the hA channel: $\mathrm{hA} \rightarrow \mathrm{b\bar{b}b\bar{b}}$ and $\mathrm{hA} \rightarrow \mathrm{b\bar{b}}\tau^+\tau^-$.

For values of m_{A} less than 30 GeV, decays of the h into a pair of A bosons become possible. The A decays predominantly to b quarks and tau leptons for most of the $\tan\beta$ region probed. The $\mathrm{hZ} \rightarrow \mathrm{b\bar{b}q\bar{q}}$ analysis has a significant cross-efficiency for the $\mathrm{hZ} \rightarrow \mathrm{AAf\bar{f}}$ channel and is used to search for this process.

Common search procedures are applied to both the hA and hZ channels. First, a preselection is applied which significantly reduces background while keeping high signal efficiency. This is especially effective against background from the two-photon interaction, which has a large cross section at these LEP energies. Second, a final set of selection cuts is chosen to distinguish signal from background. Once the final selection has been applied, a discriminating variable as defined in Reference [2, 3] is calculated for each scan point in the $(\tan\beta, m_{\mathrm{A}})$ plane.

There is a significant overlap in the selection for hA and hZ in both the channels involving either four jets, or two jets and two taus. The confidence level calculation requires that all events be uniquely assigned to a given channel. To this end, for events that pass both the hA and hZ selections, an unique assignment is made based on the reconstructed masses and the relative production rates at each scan point.

The $\mathrm{hA} \rightarrow \mathrm{b\bar{b}b\bar{b}}$ and $\mathrm{hZ} \rightarrow \mathrm{b\bar{b}q\bar{q}}$ Channels

The signature of both the $\mathrm{hA} \rightarrow \mathrm{b\bar{b}b\bar{b}}$ and $\mathrm{hZ} \rightarrow \mathrm{b\bar{b}q\bar{q}}$ decay modes is four high-multiplicity hadronic jets and the presence of b hadrons. The dominant backgrounds come from $\mathrm{q\bar{q}}$ production and hadronic decays of W pairs and Z pairs. In the case of $\mathrm{hA} \rightarrow \mathrm{b\bar{b}b\bar{b}}$, the identification of b hadrons plays an especially important role. The analysis follows closely that of Reference [3].

First, a high multiplicity hadronic preselection, common to both hA and hZ, is applied which eliminates background from the two-photon interaction. The preselection is similar to the one used at $\sqrt{s} = 183$ GeV and only minor changes are made to account for the increased center-of-mass energy. Events passing the preselection are then forced to have four jets using the DURHAM [16] clustering algorithm, and a kinematic fit requiring four-momentum conservation (4C) is performed.

Once the preselection has been satisfied, an optimization procedure is applied on the Monte Carlo to choose cuts on variables that maximize the separation between signal and background. These optimized cuts serve mainly to reject the multi-jet QCD background and are dependent on the topology being investigated: hA or hZ. Selection cuts are placed on the maximum and minimum dijet mass, minimum jet energy, maximum jet energy difference and on Y_{34}^{D}, being the value of the DURHAM jet resolution parameter for which the event is transformed from a four-jet to a three-jet topology. Values of the cuts for the hA and hZ analyses are shown in Table 1. The number of observed and expected events from Standard Model processes in the $\sqrt{s} = 189$ GeV data along with the signal efficiencies for the preselection and selection cuts are shown in Table 2.

Events passing the selection cuts are then classified in three categories: 1) those that pass only the hA cuts; 2) those that pass only the hZ cuts; and 3) those that pass both sets of cuts. Category 3) is then split into two separate samples by choosing the most likely hypothesis based on the relative production rate for hA and hZ and the probability of the mass χ^2 as defined in Reference [3].

In the final step, the analysis is optimized for four regions in the $(\tan\beta, m_{\mathrm{h}})$ plane near the limit of our discovery potential. For this, the B_{tag} variable (Figure 1a), the Higgs production angle with respect to the beam axis, Θ, (Figure 1b) and the probability for the χ^2 of the Higgs mass hypothesis (Figure 1c) are used. The relative discriminating power of these variables changes with the Higgs mass hypothesis. For this reason, a cut optimization is performed at four points in the $(\tan\beta, m_{\mathrm{h}})$ plane: (2.7,95 GeV), (7.5,80 GeV), (20,80 GeV) and (50,80 GeV).

The final discriminating variable is the logarithm of the weighted combination of the probabilities of the B_{tag} and the mass χ^2 to be consistent with background. Distributions of the final discriminant for the hA search and the hZ search are shown in Figure 2.

The $\mathrm{hZ} \rightarrow \mathrm{AAf\bar{f}}$ Channel

To investigate h decays into A-pairs in the region of very low $\tan\beta$ and low m_{A}, where this channel becomes dominant, the hZ four jet analysis described above is employed. The signature of this process is at least four hadronic jets with very high probabilities to contain b quarks. The preselection and optimized cuts chosen for the four jet analysis are applied without adjustment. The efficiency on $\mathrm{hZ} \rightarrow \mathrm{AAZ} \rightarrow \mathrm{b\bar{b}b\bar{b}q\bar{q}}$ is above 40% over the region of interest. The mass χ^2 of the four jet analysis is less effective in the six jet topology, however the B_{tag} gives the final variable enough discriminating power to distinguish between signal and background.

The $\mathrm{hA} \rightarrow \mathrm{b\bar{b}}\tau^+\tau^-$, $\mathrm{hZ} \rightarrow \mathrm{b\bar{b}}\tau^+\tau^-$ and $\mathrm{hZ} \rightarrow \tau^+\tau^-\mathrm{q\bar{q}}$ Channels

The signatures of $\mathrm{hA} \rightarrow \mathrm{b\bar{b}}\tau^+\tau^-$, $\mathrm{hZ} \rightarrow \mathrm{b\bar{b}}\tau^+\tau^-$ or $\mathrm{hZ} \rightarrow \tau^+\tau^-\mathrm{q\bar{q}}$ events[1)] are a pair of taus accompanied by two hadronic jets. The main background comes from W-pair decays containing taus. Two analyses are optimized for the hZ and for the hA channels. The hZ analysis follows that of the Standard Model Higgs search and is described in detail in Reference [2]. The $\mathrm{hA} \rightarrow \mathrm{b\bar{b}}\tau^+\tau^-$ selection is described in this letter. As in the Standard Model Higgs search, two selections are performed, one based on the tau identification (particle-based selection) and the other relying more on the event kinematics (jet-based selection).

First a common preselection is applied to both analyses, then cuts specific to each analysis are chosen. The major difference in the hA selection from that of the hZ analysis is the need for greater sensitivity to lower Higgs masses. To accomplish this, the cuts on opening angles of the jet and tau pairs have been removed, and the invariant mass cuts on the tau-tau and jet-jet systems have been relaxed. To reject the increased background accepted by loosening the selection, additional cuts are applied which exploit the kinematics of the hA events. A cut is placed on the ratio of the sum of the energies of the tau decay products to the sum of the jet energies. The magnitude of the missing momentum vector in the rest frame of the Higgs is restricted, where the taus are expected to be back-to-back resulting in a partial cancellation of the missing momentum vectors. Finally, there is a requirement on the cosine of the production angle of the Higgs boson with respect to the beam axis similar to that in the four-jet hA

[1)] The $\mathrm{hA} \rightarrow \tau^+\tau^-\mathrm{b\bar{b}}$ is also considered.

analysis. The selection cuts chosen for both the particle- and jet-based selections are shown in Table 3. The number of events observed, the number expected from background processes, and the signal efficiency for the hA and hZ analyses, after combining the particle- and jet-based selections, are shown in Table 4.

The final variable is the likelihood of the event to be hA or hZ based on the B_{tag} values for each hadronic jet, shown in Figures 3a and 3b, and the reconstructed invariant mass of either the jet or tau system, shown in Figures 3c and 3d, using the same technique as in the Standard Model Higgs search. Events which pass the hA as well as the hZ selection are classified as either hA or hZ depending on the cross section weighted values of these likelihoods. Examples of the final variable for the hA search at large values of $\tan\beta$ and the hZ search at low values of $\tan\beta$ are shown in Figure 4.

Results

No evidence of the production of the h and A bosons is observed in the data. The excluded region of the MSSM parameter space is evaluated by calculating the confidence level (CL) that the expected signal is absent in the observed data for the plane defined by $(\tan\beta, m_{\mathrm{A}})$. The CL is calculated using the technique described in References [17, 18]. Bins of an analysis with a signal-over-background ratio in the Monte Carlo of less than 0.05 are not considered in the calculation of CL. This cut is chosen to minimize the effect of systematic errors on the average CL as calculated from a large set of Monte Carlo trials.

Systematic errors on the signal and background are considered using the same procedure as in the Standard Model Higgs searches [2, 17, 19]. The overall systematic error is estimated to be 5% on the number of signal and 10% on the number of background events. Statistical uncertainties due to Monte Carlo statistics are completely uncorrelated among the different bins of the individual channels and have little effect on the final CL calculation.

The data from the MSSM Higgs search using lower center-of-mass energies [3] is combined with the $\sqrt{s}$ = 189 GeV data. Figure 5 shows the region of the $(\tan\beta, m_{\mathrm{h}})$ plane and the $(\tan\beta, m_{\mathrm{A}})$ plane excluded by L3 for the maximal and minimal mixing scenarios. On the plot, the 95% CL is shown as a solid line while the expected median CL is shown as a dashed line. Table 5 lists the masses of the h and A excluded at the 95% CL using the data at $\sqrt{s}$ = 189 GeV and lower center-of-mass energies for $\tan\beta = 3$ and $\tan\beta = 50$ as well as the median and average exclusion and the probability to obtain a higher limit. The probability to obtain a higher limit reaches a maximum in the high $\tan\beta$ region with an m_{h} mass of 68 GeV, where there is an upward fluctuation in the data. The lowest value of m_{h} excluded is at $\tan\beta = 15.0$ for maximal mixing and the lowest value of m_{A} is excluded at $\tan\beta = 50.0$ for minimal mixing. An interesting feature of these results is that the region of $0.8 < \tan\beta < 1.5$ is excluded in the MSSM, according to the current theoretical calculation of the maximum Higgs mass allowed and for m_{top} equal to 175 GeV [6]. However, recent two-loop calculations [20] seem to favor larger values of the maximum allowed m_{h} in this region, which would change the excluded band of $\tan\beta$.

For the MSSM parameters considered and assuming $\tan\beta$ greater than one, this results in lower mass limits at the 95% CL of

$$m_{\mathrm{h}} > 77.1 \text{ GeV}, \quad m_{\mathrm{A}} > 77.1 \text{ GeV}.$$

Acknowledgements

We acknowledge the efforts of the engineers and technicians who have participated in the construction and maintenance of L3 and express our gratitude to the CERN accelerator divisions for the superb performance of LEP.

References

[1] H. P. Nilles, Phys. Rep. **110** (1984) 1.
H. E. Haber and G. L. Kane, Phys. Rep. **117** (1985) 75.
R. Barbieri, Riv. Nuovo Cim. **11 n°4** (1988) 1.

[2] M. Acciarri *et al.*, Phys. Lett. **B 461** (1999) 376.

[3] L3 Collaboration, M. Acciarri *et al.*, Phys. Lett. **B 436** (1998) 389.

[4] OPAL Collaboration, G. Abbiendi *et al.*, Eur. Phys. Jo. **C 7** (1999) 407.
ALEPH Collaboration, R. Barate *et al.*, Phys. Lett. **B 440** (1998) 419.
DELPHI Collaboration, P. Abreu *et al.*, "Search for neutral Higgs bosons in e^+e^- collisions at $\sqrt{s} = 183$ GeV", Preprint EP/99-006, CERN, 1999, Submitted to E. Phys. J. **C**.

[5] L3 Collaboration, B. Adeva *et al.*, Nucl. Inst. Meth. **A 289** (1990) 35.
J. A. Bakken *et al.*, Nucl. Inst. Meth. **A 275** (1989) 81.
O. Adriani *et al.*, Nucl. Inst. Meth. **A 302** (1991) 53.
B. Adeva *et al.*, Nucl. Inst. Meth. **A 323** (1992) 109.
K. Deiters *et al.*, Nucl. Inst. Meth. **A 323** (1992) 162.
M. Chemarin *et al.*, Nucl. Inst. Meth. **A 349** (1994) 345.
M. Acciarri *et al.*, Nucl. Inst. Meth. **A 351** (1994) 300.
G. Basti *et al.*, Nucl. Inst. Meth. **A 374** (1996) 293.
A. Adam *et al.*, Nucl. Inst. Meth. **A 383** (1996) 342.

[6] P. Janot, The HZHA Generator, in *Physics at LEP2*, edited by G. Altarelli, T. Sjöstrand, and F. Zwirner, page 309, Geneva, Switzerland, 1996, CERN, CERN 96-01.

[7] T. Sjöstrand, "PYTHIA", Preprint TH/93-7112, CERN, 1993, Revised August 1995.
T. Sjöstrand, Comp. Phys. Comm. **82** (1994) 74.

[8] M. Skrzypek *et al.*, Comp. Phys. Comm. **94** (1996) 216.
M. Skrzypek *et al.*, Phys. Lett. **B 372** (1996) 289.

[9] S. Jadach, B. F. L. Ward, and Z. Wąs, Comp. Phys. Comm. **66** (1991) 276.

[10] R. Engel, Z. Phys. **C 66** (1995) 203.
R. Engel, J. Ranft, and S. Roesler, Phys. Rev. **D 52** (1995) 1459.

[11] F. A. Berends, R. Pittau, and R. Kleiss, Comp. Phys. Comm. **85** (1995) 437.

[12] R. Brun *et al.*, "GEANT 3", CERN DD/EE/84-1, Revised 1987.

[13] H. Fesefeldt, "GHEISHA", Preprint PITHA 85/02, RWTH Aachen, 1985.

[14] M. Carena and P. M. Zerwas, Higgs Physics, in *Physics at LEP2*, edited by G. Altarelli, T. Sjöstrand, and F. Zwirner, page 351, Geneva, Switzerland, 1996, CERN, CERN 96-01.

[15] OPAL Collaboration, G. Alexander *et al.*, Z. Phys. **C 73** (1997) 189.

[16] S. Bethke *et al.*, Nucl. Phys. **B 370** (1992) 310.

[17] L3 Collaboration, M. Acciarri *et al.*, Phys. Lett. **B 411** (1997) 373.

[18] A. Favara and M. Pieri, "Confidence Level Estimation and Analysis Optimization", Preprint, INFN University of Florence, 1997, DFF-278-4-1997.

[19] L3 Collaboration, M. Acciarri *et al.*, Phys. Lett. **B 431** (1998) 437.

[20] S. Heinemeyer, W. Hollik, and G. Weiglein, Phys. Lett. **B 440** (1998) 296.

The L3 Collaboration:

M.Acciarri,[26] P.Achard,[19] O.Adriani,[16] M.Aguilar-Benitez,[25] J.Alcaraz,[25] G.Alemanni,[22] J.Allaby,[17] A.Aloisio,[28] M.G.Alviggi,[28] G.Ambrosi,[19] H.Anderhub,[47] V.P.Andreev,[6,36] T.Angelescu,[12] F.Anselmo,[9] A.Arefiev,[27] T.Azemoon,[3] T.Aziz,[10] P.Bagnaia,[35] L.Baksay,[42] A.Balandras,[4] R.C.Ball,[3] S.Banerjee,[10] Sw.Banerjee,[10] A.Barczyk,[47,45] R.Barillère,[17] L.Barone,[35] P.Bartalini,[22] M.Basile,[9] R.Battiston,[32] A.Bay,[22] F.Becattini,[16] U.Becker,[14] F.Behner,[47] L.Bellucci,[16] J.Berdugo,[25] P.Berges,[14] B.Bertucci,[32] B.L.Betev,[47] S.Bhattacharya,[10] M.Biasini,[32] A.Biland,[47] J.J.Blaising,[4] S.C.Blyth,[33] G.J.Bobbink,[2] A.Böhm,[1] L.Boldizsar,[13] B.Borgia,[35] D.Bourilkov,[47] M.Bourquin,[19] S.Braccini,[19] J.G.Branson,[38] V.Brigljevic,[47] F.Brochu,[4] A.Buffini,[16] A.Buijs,[43] J.D.Burger,[14] W.J.Burger,[32] J.Busenitz,[42] A.Button,[3] X.D.Cai,[14] M.Campanelli,[47] M.Capell,[14] G.Cara Romeo,[9] G.Carlino,[28] A.M.Cartacci,[16] J.Casaus,[25] G.Castellini,[16] F.Cavallari,[35] N.Cavallo,[28] C.Cecchi,[19] M.Cerrada,[25] F.Cesaroni,[23] M.Chamizo,[19] Y.H.Chang,[49] U.K.Chaturvedi,[18] M.Chemarin,[24] A.Chen,[49] G.Chen,[7] G.M.Chen,[7] H.F.Chen,[20] H.S.Chen,[7] X.Chereau,[4] G.Chiefari,[28] L.Cifarelli,[37] F.Cindolo,[9] C.Civinini,[16] I.Clare,[14] R.Clare,[14] G.Coignet,[4] A.P.Colijn,[2] N.Colino,[25] S.Costantini,[8] F.Cotorobai,[12] B.Cozzoni,[9] B.de la Cruz,[25] A.Csilling,[13] S.Cucciarelli,[32] T.S.Dai,[14] J.A.van Dalen,[30] R.D'Alessandro,[16] R.de Asmundis,[28] P.Déglon,[19] A.Degré,[4] K.Deiters,[45] D.della Volpe,[28] P.Denes,[34] F.DeNotaristefani,[35] A.De Salvo,[47] M.Diemoz,[35] D.van Dierendonck,[2] F.Di Lodovico,[47] C.Dionisi,[35] M.Dittmar,[47] A.Dominguez,[38] A.Doria,[28] M.T.Dova,[18,♯] D.Duchesneau,[4] D.Dufournaud,[4] P.Duinker,[2] I.Duran,[39] H.El Mamouni,[24] A.Engler,[33] F.J.Eppling,[14] F.C.Erné,[2] P.Extermann,[19] M.Fabre,[45] R.Faccini,[35] M.A.Falagan,[25] S.Falciano,[35,17] A.Favara,[17] J.Fay,[24] O.Fedin,[36] M.Felcini,[47] T.Ferguson,[33] F.Ferroni,[35] H.Fesefeldt,[1] E.Fiandrini,[32] J.H.Field,[19] F.Filthaut,[17] P.H.Fisher,[14] I.Fisk,[38] G.Forconi,[14] L.Fredj,[19] K.Freudenreich,[47] C.Furetta,[26] Yu.Galaktionov,[27,14] S.N.Ganguli,[10] P.Garcia-Abia,[5] M.Gataullin,[31] S.S.Gau,[11] S.Gentile,[35,17] N.Gheordanescu,[12] S.Giagu,[35] Z.F.Gong,[20] G.Grenier,[24] O.Grimm,[47] M.W.Gruenewald,[8] M.Guida,[37] R.van Gulik,[2] V.K.Gupta,[34] A.Gurtu,[10] L.J.Gutay,[44] D.Haas,[5] A.Hasan,[29] D.Hatzifotiadou,[9] T.Hebbeker,[8] A.Hervé,[17] P.Hidas,[13] J.Hirschfelder,[33] H.Hofer,[47] G. Holzner,[47] H.Hoorani,[33] S.R.Hou,[49] I.Iashvili,[46] B.N.Jin,[7] L.W.Jones,[3] P.de Jong,[2] I.Josa-Mutuberría,[25] R.A.Khan,[18] D.Kamrad,[46] M.Kaur,[18,◇] M.N.Kienzle-Focacci,[19] D.Kim,[35] D.H.Kim,[41] J.K.Kim,[41] S.C.Kim,[41] J.Kirkby,[17] D.Kiss,[13] W.Kittel,[30] A.Klimentov,[14,27] A.C.König,[30] A.Kopp,[46] V.Koutsenko,[14,27] M.Kräber,[47] R.W.Kraemer,[33] W.Krenz,[1] A.Kunin,[14,27] P.Ladron de Guevara,[25] I.Laktineh,[24] G.Landi,[16] K.Lassila-Perini,[47] P.Laurikainen,[21] M.Lebeau,[17] A.Lebedev,[14] P.Lebrun,[24] P.Lecomte,[47] P.Lecoq,[17] P.Le Coultre,[47] H.J.Lee,[8] J.M.Le Goff,[17] R.Leiste,[46] E.Leonardi,[35] P.Levtchenko,[36] C.Li,[20] C.H.Lin,[49] W.T.Lin,[49] F.L.Linde,[2] L.Lista,[28] Z.A.Liu,[7] W.Lohmann,[46] E.Longo,[35] Y.S.Lu,[7] K.Lübelsmeyer,[1] C.Luci,[17,35] D.Luckey,[14] L.Lugnier,[24] L.Luminari,[35] W.Lustermann,[47] W.G.Ma,[20] M.Maity,[10] L.Malgeri,[17] A.Malinin,[27,17] C.Maña,[25] D.Mangeol,[30] P.Marchesini,[47] G.Marian,[15] J.P.Martin,[24] F.Marzano,[35] G.G.G.Massaro,[2] K.Mazumdar,[10] R.R.McNeil,[6] S.Mele,[17] L.Merola,[28] M.Meschini,[16] W.J.Metzger,[30] M.von der Mey,[1] A.Mihul,[12] H.Milcent,[17] G.Mirabelli,[35] J.Mnich,[17] G.B.Mohanty,[10] P.Molnar,[8] B.Monteleoni,[16,†] T.Moulik,[10] G.S.Muanza,[24] F.Muheim,[19] A.J.M.Muijs,[2] M.Musy,[35] M.Napolitano,[28] F.Nessi-Tedaldi,[47] H.Newman,[31] T.Niessen,[1] A.Nisati,[35] H.Nowak,[46] Y.D.Oh,[41] G.Organtini,[35] R.Ostonen,[21] A.Oulianov,[27] C.Palomares,[25] D.Pandoulas,[1] S.Paoletti,[35,17] P.Paolucci,[28] R.Paramatti,[35] H.K.Park,[33] I.H.Park,[41] G.Pascale,[35] G.Passaleva,[17] S.Patricelli,[28] T.Paul,[11] M.Pauluzzi,[32] C.Paus,[17] F.Pauss,[47] D.Peach,[17] M.Pedace,[35] S.Pensotti,[26] D.Perret-Gallix,[4] B.Petersen,[30] D.Piccolo,[28] F.Pierella,[9] M.Pieri,[16] P.A.Piroué,[34] E.Pistolesi,[26] V.Plyaskin,[27] M.Pohl,[47] V.Pojidaev,[27,16] H.Postema,[14] J.Pothier,[17] N.Produit,[19] D.O.Prokofiev,[44] D.Prokofiev,[36] J.Quartieri,[37] G.Rahal-Callot,[47,17] M.A.Rahaman,[10] P.Raics,[15] N.Raja,[10] R.Ramelli,[47] P.G.Rancoita,[26] G.Raven,[38] P.Razis,[29] D.Ren,[47] M.Rescigno,[35] S.Reucroft,[11] T.van Rhee,[43] S.Riemann,[46] K.Riles,[3] A.Robohm,[47] J.Rodin,[42] B.P.Roe,[3] L.Romero,[25] A.Rosca,[8] S.Rosier-Lees,[4] J.A.Rubio,[17] D.Ruschmeier,[8] H.Rykaczewski,[47] S.Saremi,[6] S.Sarkar,[35] J.Salicio,[17] E.Sanchez,[17] M.P.Sanders,[30] M.E.Sarakinos,[21] C.Schäfer,[1] V.Schegelsky,[36] S.Schmidt-Kaerst,[1] D.Schmitz,[1] H.Schopper,[48] D.J.Schotanus,[30] G.Schwering,[1] C.Sciacca,[28] D.Sciarrino,[19] A.Seganti,[9] L.Servoli,[32] S.Shevchenko,[31] N.Shivarov,[40] V.Shoutko,[27] E.Shumilov,[27] A.Shvorob,[31] T.Siedenburg,[1] D.Son,[41] B.Smith,[33] P.Spillantini,[16] M.Steuer,[14] D.P.Stickland,[34] A.Stone,[6] H.Stone,[34,†] B.Stoyanov,[40] A.Straessner,[1] K.Sudhakar,[10] G.Sultanov,[18] L.Z.Sun,[20] H.Suter,[47] J.D.Swain,[18] Z.Szillasi,[42,¶] T.Sztaricskai,[42,¶] X.W.Tang,[7] L.Tauscher,[5] L.Taylor,[11] C.Timmermans,[30] Samuel C.C.Ting,[14] S.M.Ting,[14] S.C.Tonwar,[10] J.Tóth,[13] C.Tully,[34] K.L.Tung,[7] Y.Uchida,[14] J.Ulbricht,[47] E.Valente,[35] G.Vesztergombi,[13] I.Vetlitsky,[27] D.Vicinanza,[37] G.Viertel,[47] S.Villa,[11] M.Vivargent,[4] S.Vlachos,[5] I.Vodopianov,[36] H.Vogel,[33] H.Vogt,[46] I.Vorobiev,[27] A.A.Vorobyov,[36] A.Vorvolakos,[29] M.Wadhwa,[5] W.Wallraff,[1] M.Wang,[14] X.L.Wang,[20] Z.M.Wang,[20] A.Weber,[1] M.Weber,[1] P.Wienemann,[1] H.Wilkens,[30] S.X.Wu,[14] S.Wynhoff,[1] L.Xia,[31] Z.Z.Xu,[20] B.Z.Yang,[20] C.G.Yang,[7] H.J.Yang,[7] M.Yang,[7] J.B.Ye,[20] S.C.Yeh,[50] An.Zalite,[36] Yu.Zalite,[36] Z.P.Zhang,[20] G.Y.Zhu,[7] R.Y.Zhu,[31] A.Zichichi,[9,17,18] F.Ziegler,[46] G.Zilizi,[42,¶] M.Zöller.[1]

1 I. Physikalisches Institut, RWTH, D-52056 Aachen, FRG[§]
III. Physikalisches Institut, RWTH, D-52056 Aachen, FRG[§]
2 National Institute for High Energy Physics, NIKHEF, and University of Amsterdam, NL-1009 DB Amsterdam, The Netherlands
3 University of Michigan, Ann Arbor, MI 48109, USA
4 Laboratoire d'Annecy-le-Vieux de Physique des Particules, LAPP,IN2P3-CNRS, BP 110, F-74941 Annecy-le-Vieux CEDEX, France
5 Institute of Physics, University of Basel, CH-4056 Basel, Switzerland
6 Louisiana State University, Baton Rouge, LA 70803, USA
7 Institute of High Energy Physics, IHEP, 100039 Beijing, China[△]
8 Humboldt University, D-10099 Berlin, FRG[§]
9 University of Bologna and INFN-Sezione di Bologna, I-40126 Bologna, Italy
10 Tata Institute of Fundamental Research, Bombay 400 005, India
11 Northeastern University, Boston, MA 02115, USA
12 Institute of Atomic Physics and University of Bucharest, R-76900 Bucharest, Romania
13 Central Research Institute for Physics of the Hungarian Academy of Sciences, H-1525 Budapest 114, Hungary[‡]
14 Massachusetts Institute of Technology, Cambridge, MA 02139, USA
15 KLTE-ATOMKI, H-4010 Debrecen, Hungary[¶]
16 INFN Sezione di Firenze and University of Florence, I-50125 Florence, Italy
17 European Laboratory for Particle Physics, CERN, CH-1211 Geneva 23, Switzerland
18 World Laboratory, FBLJA Project, CH-1211 Geneva 23, Switzerland
19 University of Geneva, CH-1211 Geneva 4, Switzerland
20 Chinese University of Science and Technology, USTC, Hefei, Anhui 230 029, China[△]
21 SEFT, Research Institute for High Energy Physics, P.O. Box 9, SF-00014 Helsinki, Finland
22 University of Lausanne, CH-1015 Lausanne, Switzerland
23 INFN-Sezione di Lecce and Universitá Degli Studi di Lecce, I-73100 Lecce, Italy
24 Institut de Physique Nucléaire de Lyon, IN2P3-CNRS,Université Claude Bernard, F-69622 Villeurbanne, France
25 Centro de Investigaciones Energéticas, Medioambientales y Tecnologícas, CIEMAT, E-28040 Madrid, Spain♭
26 INFN-Sezione di Milano, I-20133 Milan, Italy
27 Institute of Theoretical and Experimental Physics, ITEP, Moscow, Russia
28 INFN-Sezione di Napoli and University of Naples, I-80125 Naples, Italy
29 Department of Natural Sciences, University of Cyprus, Nicosia, Cyprus
30 University of Nijmegen and NIKHEF, NL-6525 ED Nijmegen, The Netherlands
31 California Institute of Technology, Pasadena, CA 91125, USA
32 INFN-Sezione di Perugia and Universitá Degli Studi di Perugia, I-06100 Perugia, Italy
33 Carnegie Mellon University, Pittsburgh, PA 15213, USA
34 Princeton University, Princeton, NJ 08544, USA
35 INFN-Sezione di Roma and University of Rome, "La Sapienza", I-00185 Rome, Italy
36 Nuclear Physics Institute, St. Petersburg, Russia
37 University and INFN, Salerno, I-84100 Salerno, Italy
38 University of California, San Diego, CA 92093, USA
39 Dept. de Fisica de Particulas Elementales, Univ. de Santiago, E-15706 Santiago de Compostela, Spain
40 Bulgarian Academy of Sciences, Central Lab. of Mechatronics and Instrumentation, BU-1113 Sofia, Bulgaria
41 Center for High Energy Physics, Adv. Inst. of Sciences and Technology, 305-701 Taejon, Republic of Korea
42 University of Alabama, Tuscaloosa, AL 35486, USA
43 Utrecht University and NIKHEF, NL-3584 CB Utrecht, The Netherlands
44 Purdue University, West Lafayette, IN 47907, USA
45 Paul Scherrer Institut, PSI, CH-5232 Villigen, Switzerland
46 DESY, D-15738 Zeuthen, FRG
47 Eidgenössische Technische Hochschule, ETH Zürich, CH-8093 Zürich, Switzerland
48 University of Hamburg, D-22761 Hamburg, FRG
49 National Central University, Chung-Li, Taiwan, China
50 Department of Physics, National Tsing Hua University, Taiwan, China
§ Supported by the German Bundesministerium für Bildung, Wissenschaft, Forschung und Technologie
‡ Supported by the Hungarian OTKA fund under contract numbers T019181, F023259 and T024011.
¶ Also supported by the Hungarian OTKA fund under contract numbers T22238 and T026178.
♭ Supported also by the Comisión Interministerial de Ciencia y Tecnología.
♯ Also supported by CONICET and Universidad Nacional de La Plata, CC 67, 1900 La Plata, Argentina.
♢ Also supported by Panjab University, Chandigarh-160014, India.
△ Supported by the National Natural Science Foundation of China.
† Deceased.

Cut	hA	hZ
Minimum dijet mass (GeV)	> 15.7	> 25.3
Maximum dijet mass (GeV)	< 135.3	< 118.7
Minimum jet energy (GeV)	> 15.1	> 25.9
Maximum $\Delta E_{\rm jet}$ (GeV)	< 54.8	< 42.4
$Y_{34}^{\rm D}$	> 0.003	> 0.009
Visible Energy (GeV)	> 129.3	> 133.8
Number of Tracks	> 25	> 22

Table 1: Selection cuts for the hA and hZ four-jet Higgs search channels. In addition to those abbreviations defined in the text, the symbol $\Delta E_{\rm jet}$ is the energy difference between any two jets of the four-jet system.

Process	Number of Events Preselection	hA cuts	hZ cuts
$e^+e^- \to e^+e^- q\bar{q}$	7.1	0.7	0.6
$e^+e^- \to q\bar{q}$	758.0	203.7	57.4
$e^+e^- \to W^+W^-$	1331.7	913.5	582.1
$e^+e^- \to ZZ$	76.0	47.5	37.6
Total Expected	2172.8	1165.4	677.7
Data	2141	1110	641
Efficiency $hA \to b\bar{b}b\bar{b}$	91.5%	77.1%	43.6%
Efficiency $hZ \to b\bar{b}q\bar{q}$	93.3%	78.2%	66.2%

Table 2: Number of events expected and observed in the four-jets channels. The signal efficiencies at $\sqrt{s} = 189$ GeV are quoted for hA at $m_A = m_h = 80$ GeV and for hZ at $m_h = 95$ GeV.

Cut	Particle-based selection	Jet-based selection
Number of tracks	≥ 5	≥ 5
Number of clusters	≥ 15	≥ 15
$E_{\mathrm{vis}}/\sqrt{s}$	≥ 0.4, ≤ 0.95	≥ 0.4, ≤ 0.90
E_{e},E_{μ},E_{γ}	≤ 40 GeV	≤ 40 GeV
$\ln Y_{34}^{\mathrm{D}}$	$\geq$ -6	$\geq$ -6
E^{τ}	≤ 1	≤ 1
$m_{\tau\tau}$,m_{qq}	≥ 5 GeV,≤ 125 GeV	≥ 5 GeV,≤ 125 GeV
$\mid \cos\Theta \mid$	≤ 0.8	≤ 0.8
$\mid p^{*}_{\mathrm{miss}} \mid$	≤ 40 GeV	≤ 40 GeV
$\mid \cos(\Theta_{\mathrm{miss}}) \mid$	-	≤ 0.95
$\alpha_{\tau\text{-jet}}$	-	$\geq 25^{\circ}$

Table 3: Selection cuts for particle-based and jet-based tau selections in the $\mathrm{hA} \to \mathrm{b\bar{b}}\tau^{+}\tau^{-}$ search channel. In addition to those abbreviations defined in the text: E_{vis} is the visible energy; E_{e}, E_{μ} and E_{γ} are the electron, muon and photon energies, respectively; E^{τ} is the ratio of the sum of the energies of the tau decay products to the sum of the jet energies; $m_{\tau\tau}$,m_{qq} is the invariant mass of the tau-tau and jet-jet systems, respectively; Θ is the production angle of the Higgs boson with respect to the beam axis; p^{*}_{miss} is the magnitude of the missing momentum vector in the rest frame of the Higgs; Θ_{miss} is the angle of missing energy vector with respect to the beam axis; and $\alpha_{\tau\text{-jet}}$ is the angle between a tau jet and the closest quark jet.

Process	Number of Events hA selection	hZ selection
$e^+e^- \to q\bar{q}$	2.3	2.3
$e^+e^- \to W^+W^-$	11.3	11.2
$e^+e^- \to ZZ$	2.6	3.1
$e^+e^- \to Ze^+e^-$	0.4	0.5
Total Expected	16.6	17.1
Data	20	12
Efficiency $hA \to b\bar{b}\tau^+\tau^-$	35.2%	35.4%
Efficiency $hZ \to b\bar{b}\tau^+\tau^-$	21.1%	30.0%
Efficiency $hZ \to \tau^+\tau^- q\bar{q}$	21.8%	29.8%

Table 4: Number of events expected and observed after selection for the tau search channels. The signal efficiencies at $\sqrt{s} = 189$ GeV are quoted for hA at $m_A = m_h = 80$ GeV and for hZ at $m_h = 95$ GeV.

	Lower mass limits in GeV at 95% *CL*						
	Observed		Expected				
Mixing, tanβ	$\boldsymbol{m_{\mathrm{h}}}$	$\boldsymbol{m_{\mathrm{A}}}$	$<m_{\mathrm{h}}>$	$<m_{\mathrm{A}}>$	$\overline{m}_{\mathrm{h}}$	$\overline{m}_{\mathrm{A}}$	CL_b
minimal, 3	**96.3**	**225.0**	92.7	164.0	94.6	192.6	12%
minimal, 50	**77.1**	**77.1**	78.2	78.2	80.0	80.0	80%
maximal, 3	**95.4**	**128.9**	89.0	111.9	90.4	117.1	15%
maximal, 50	**77.5**	**77.6**	78.9	79.0	81.4	81.5	77%

Table 5: Higgs mass limits in the MSSM from the data at $\sqrt{s}$ = 130 GeV − 189 GeV. The masses in boldface are the lower mass limits set at the 95% *CL* from the data. The masses $<m>$ and $\overline{m}$ are respectively the average and median mass limits for the h and A bosons as calculated from a large set of Monte Carlo trials. Assuming there is no signal, CL_b is the probability to obtain a mass limit on m_{h} larger than the one observed.

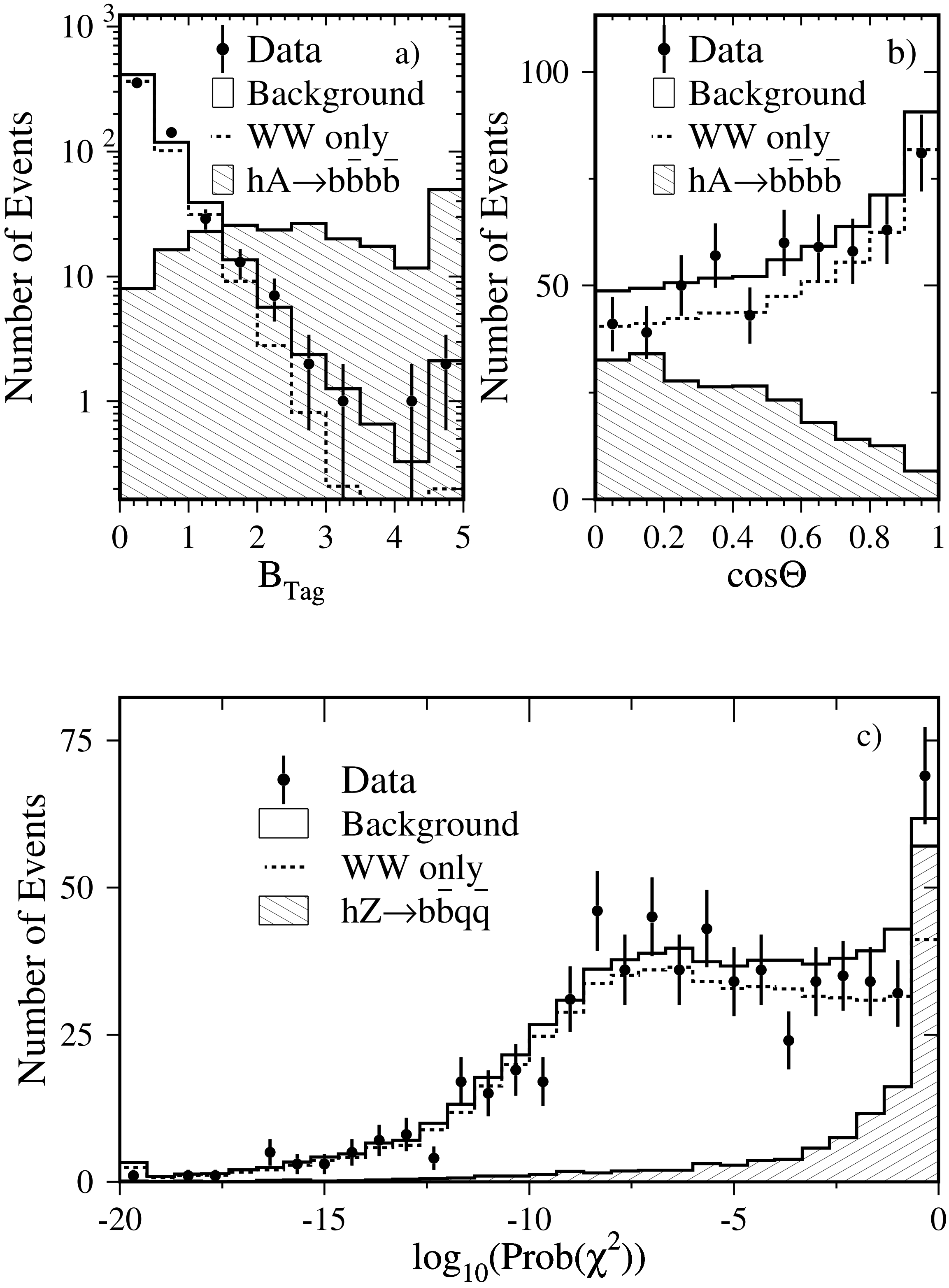

Figure 1: Distributions of the a) B_{tag} and b) cosine of the Higgs production angle Θ in the four-jets search. The hatched histogram is the expected hA signal (multiplied by a factor of 50) for $m_{\mathrm{h}} = 80$ GeV and $\tan\beta = 50$. Distribution c) is the logarithm of the probability of the mass χ^2. The hatched histogram is the expected hZ signal (multiplied by a factor of 10) for $m_{\mathrm{h}} = 95$ GeV and $\tan\beta = 3$.

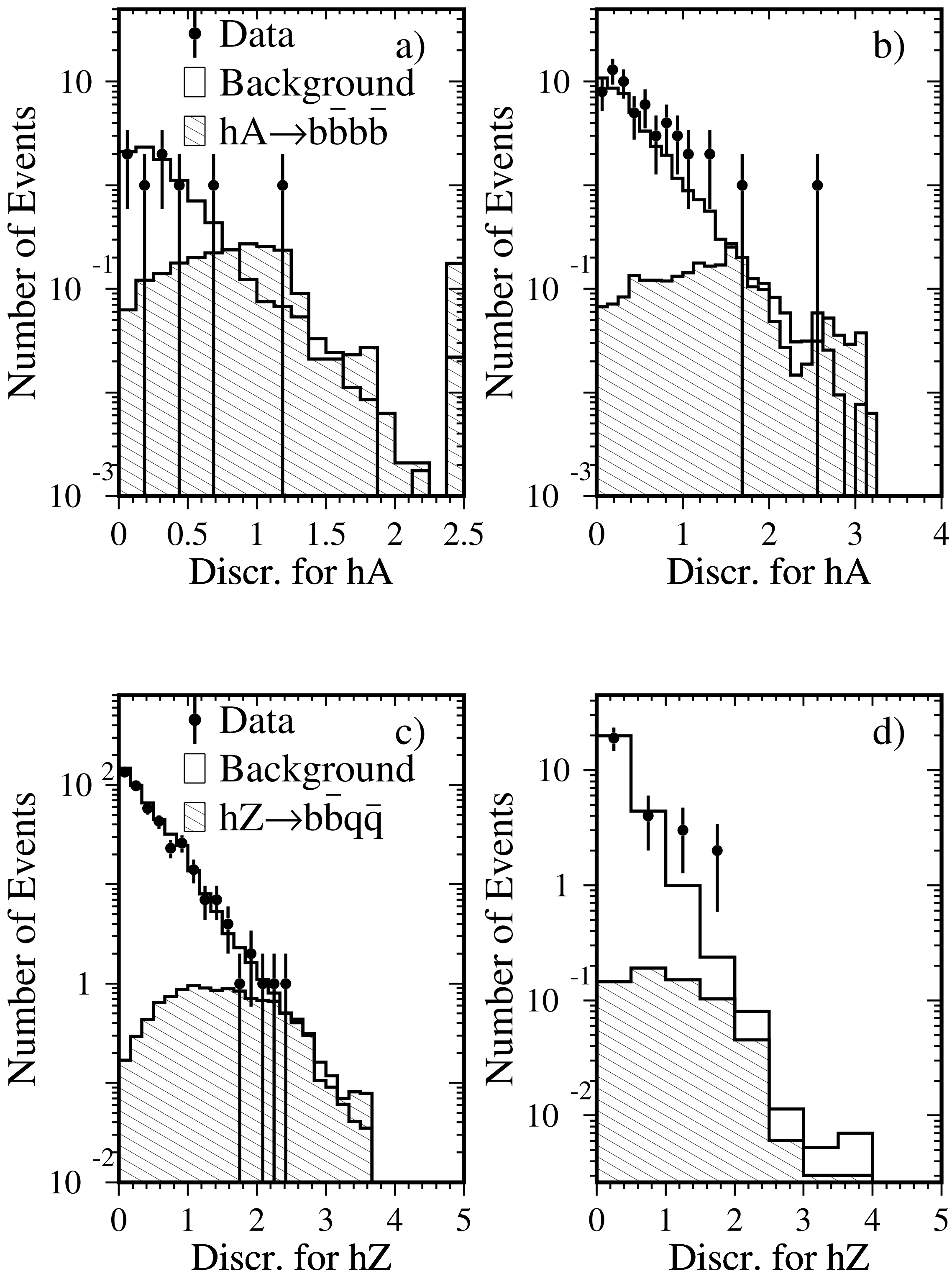

Figure 2: Distributions of the final discriminant for the category of events passing a) both hA and hZ cuts but classified as hA candidates and b) events passing only the set of cuts for hA. The hatched histogram is the hA signal expectation for $m_{\mathrm{h}} = 80$ GeV and $\tan\beta = 50$. Distributions are plotted for c) the events passing both hA and hZ cuts but classified as hZ and d) events passing only the hZ selection. The hatched histogram is the hZ signal expectation for $m_{\mathrm{h}} = 95$ GeV and $\tan\beta = 3$.

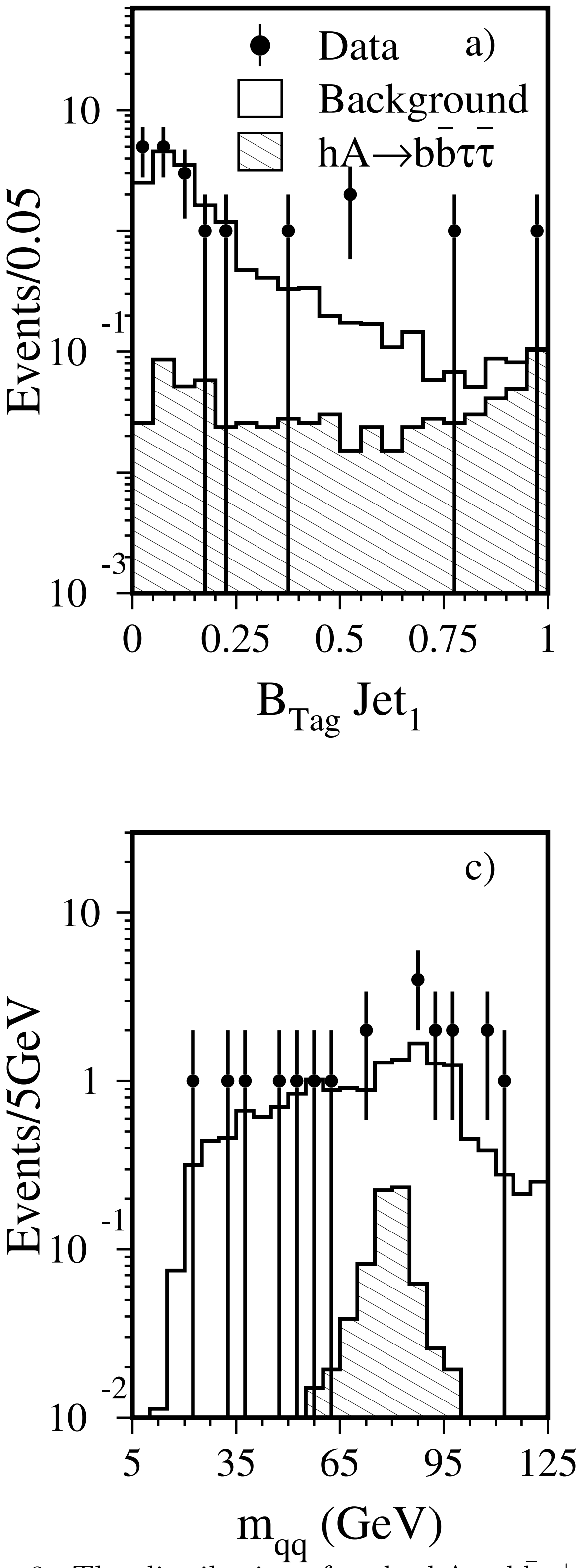

Figure 3: The distributions for the hA$\to$b$\bar{\text{b}}\tau^+\tau^-$ search channel of a) the B_{tag} for hadronic jet 1 and b) hadronic jet 2, c) the reconstructed mass for the hadronic system, and d) the reconstructed mass for the tau-tau system. The hatched histogram is the hA$\to$b$\bar{\text{b}}\tau^+\tau^-$ signal normalized for $m_{\text{h}} = 80$ GeV and $\tan\beta = 50$.

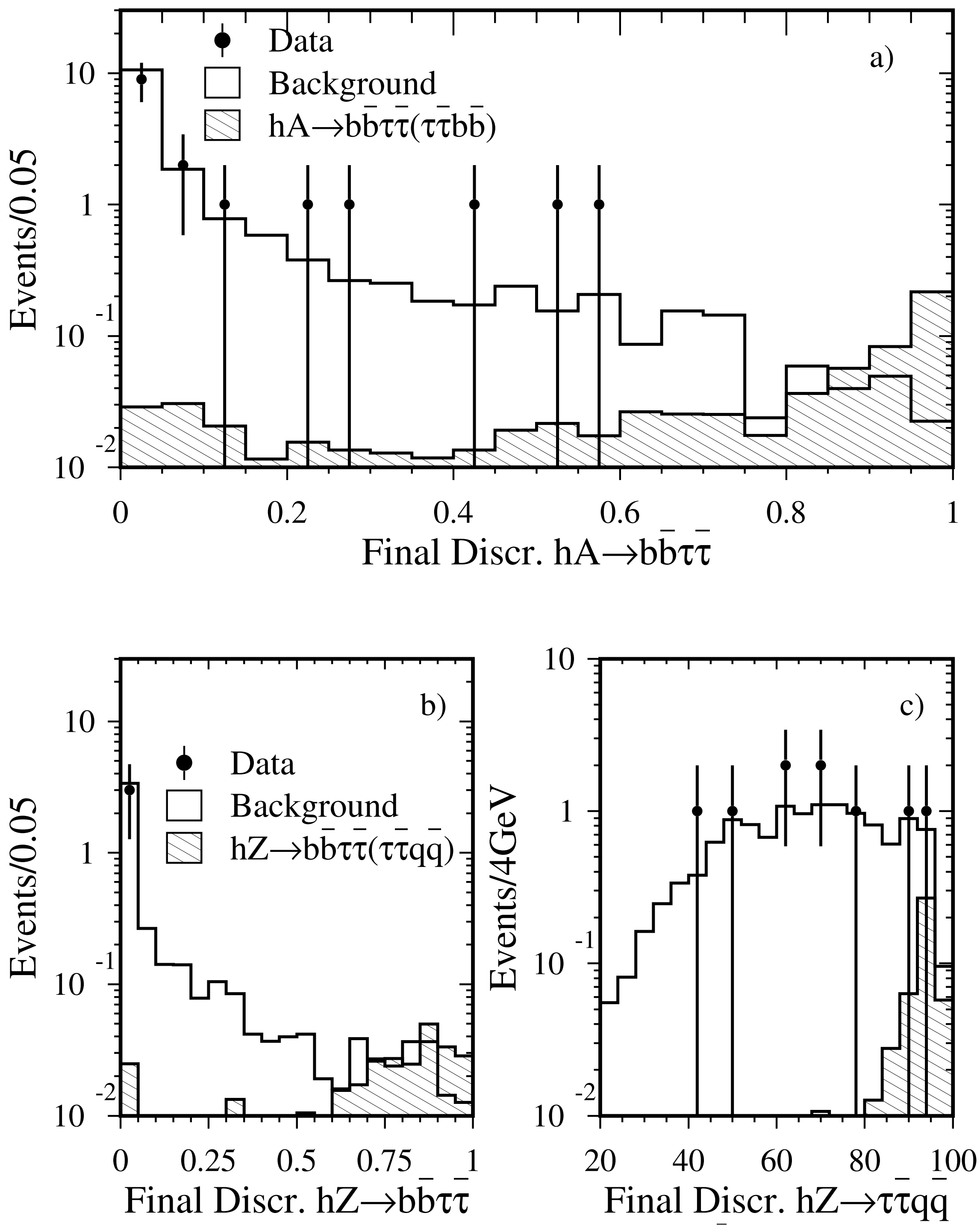

Figure 4: Distributions of the final variables for the a) $\mathrm{hA}\to\mathrm{b}\bar{\mathrm{b}}\tau^+\tau^-$ for $m_\mathrm{h} = 80$ GeV at $\tan\beta = 50$, b) the $\mathrm{hZ}\to\mathrm{b}\bar{\mathrm{b}}\tau^+\tau^-$ for $m_\mathrm{h} = 95$ GeV at $\tan\beta = 3$ and c) the $\mathrm{hZ}\to\tau^+\tau^-\mathrm{q}\bar{\mathrm{q}}$ search for $m_\mathrm{h} = 95$ GeV at $\tan\beta = 3$.

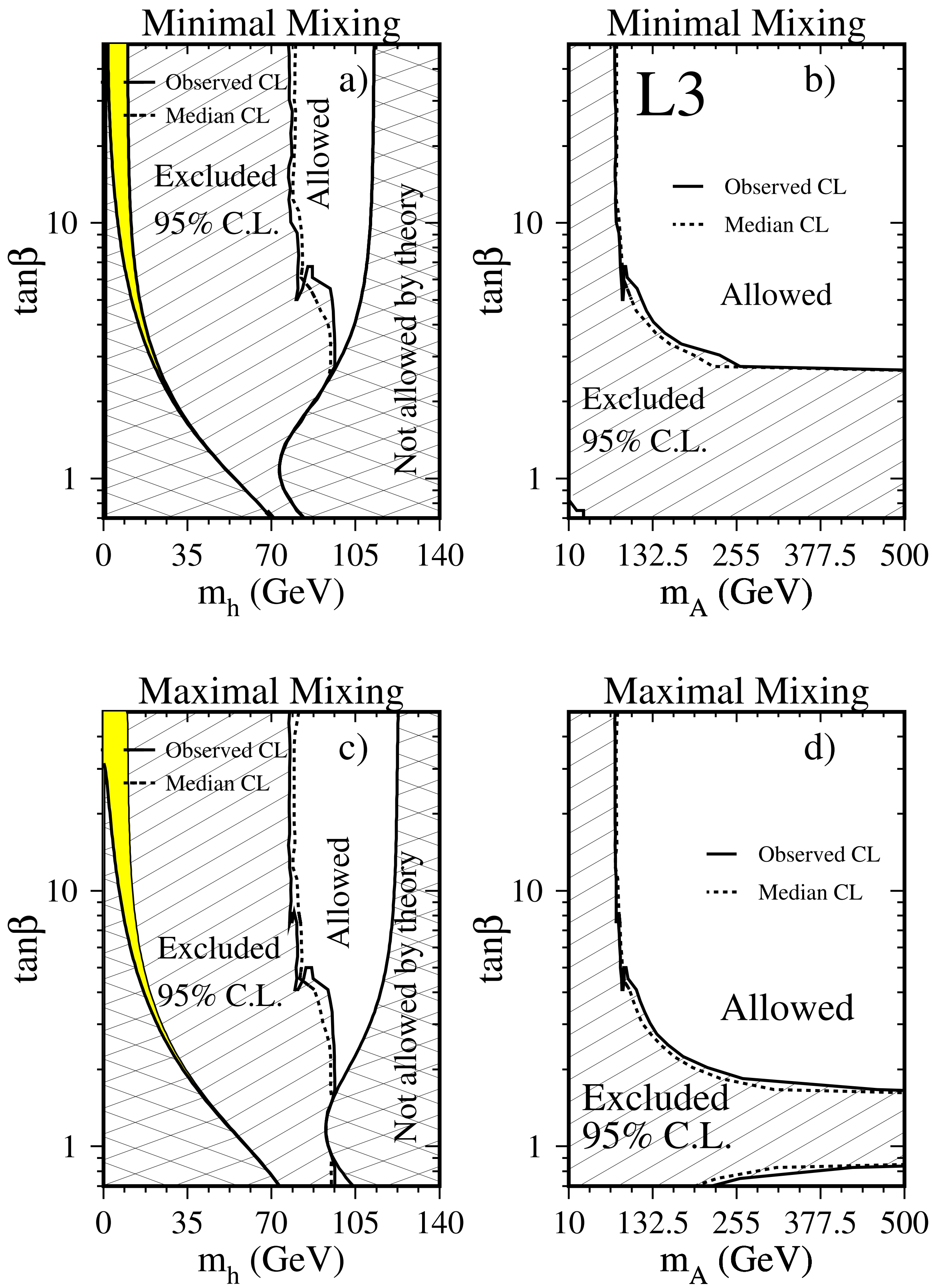

Figure 5: Exclusion plots of the Higgs mass versus tanβ at the 95% CL. In all plots the area shaded by diagonal lines is the 95% exclusion, while the cross-hatched region is theoretically disallowed. The grey region in plots a) and c) corresponds to $m_{\mathrm{A}} < 10$ GeV and has been previous excluded at LEP [15]. Plot a) is the 95% CL exclusion of m_{h} versus tanβ in the minimal mixing scenario, and b) is the 95% exclusion of m_{A} versus tanβ also for minimal mixing. Plots c) and d) are the same for the maximal mixing scenario.